IEEE Open Journal of Vehicular Technology

Received XX Month, XXXX; revised XX Month, XXXX; accepted XX Month, XXXX; Date of publication XX Month, XXXX; date of current version XX Month, XXXX.

Digital Object Identifier 10.1109/OJVT.2023.XXXXXXX

Source-Difference-Based Mapping Improves Spatial Modulation

YULI YANG[1], *SENIOR MEMBER, IEEE*, CHAO XU[2], *SENIOR MEMBER, IEEE*, AND LAJOS HANZO[2], *LIFE FELLOW, IEEE*

[1]School of Computer Science and Electronic Engineering, University of Essex, Colchester CO4 3SQ, U.K.
[2]School of Electronics and Computer Science, University of Southampton, Southampton SO17 1BJ, U.K.

CORRESPONDING AUTHOR: LAJOS HANZO (e-mail: lh@ecs.soton.ac.uk).

This paper was presented in part at the IEEE International Wireless Communications and Mobile Computing Conference (IWCMC), Dubrovnik, Croatia, May 2022 [1]. Yuli Yang would like to acknowledge the financial support of the Engineering and Physical Sciences Research Council project EP/X04047X/1. Lajos Hanzo would like to acknowledge the financial support of the Engineering and Physical Sciences Research Council projects EP/W016605/1, EP/X01228X/1 and EP/X01228X/1 as well as of the European Research Council's Advanced Fellow Grant QuantCom (Grant No. 789028).

ABSTRACT A new multi-antenna transmission scheme, referred to as difference-based spatial modulation (DBSM), is proposed to enhance the reliability of spatial modulation (SM). With the DBSM, a pair of amplitude/phase-shift keying (APSK) symbols are conveyed by each channel-use, but only one of them is radiated from a single transmit antenna. In contrast to conventional SM, DBSM selects the active transmit antenna based on the difference between the two symbols of a channel-use, rather than one of them. The design principle of the APSK constellation in the DBSM is detailed, which guarantees that the mean Euclidean distance between any two DBSM signals mapped by a pair of complementary bit-sequences is the largest possible among all the candidates. In this way, DBSM improves the error performance of conventional SM, even though they have the same achievable data rate given the same system configuration. We demonstrate that channel coding techniques, e.g., convolutional and turbo codes, will enhance the performance gain achieved by DBSM over conventional SM. Both theoretical analysis and simulation results are provided to substantiate the advantages of our proposed DBSM scheme.

INDEX TERMS Achievable data rate (ADR), bit error rate (BER), difference-based spatial modulation (DBSM), multiple-input-multiple-output (MIMO) systems, permutation modulation.

I. INTRODUCTION

While 5G services are rolled out around the world, the research focus of practitioners has evolved towards 6G networks. Aiming to provide ultra-reliable and high-rate communications at extremely low end-to-end latency in a wide range of applications, numerous physical-layer solutions have been proposed for addressing the challenges and opportunities of future wireless services [2], [3]. In this context, permutation-based modulation is a competitive concept [4], [5], which utilises the indices of activated resource units, including transmit antennas (TAs), spectral bands, time slots, channelisation codes, and polarisation states, to convey extra information bits along with the conventionally modulated symbols.

Spatial modulation (SM) is a prominent member in the permutation modulation family, which was designed for point-to-point open-loop multi-antenna configurations and enables the index of every TA to be used as an additional dimension for conveying information [6]. The delivery of the information mapped into this dimension does not consume any extra communication resource, which improves the spectral efficiency at low hardware complexity. In each transmission, the SM activates only a single TA and requires only a single radio-frequency (RF) chain. This achieves higher energy efficiency than other multi-antenna approaches, while additionally mitigating the inter-channel and/or inter-antenna interference.

The SM channel capacity was derived in [7]. Then, the achievable data rate (ADR) of SM in multiple-input-multiple-output (MIMO) systems relying on imperfect channel estimation [8] and on realistic channel state impairments [9] has been derived. Moreover, the optimal spatial-design [10] and the optimal power-allocation [11] have been developed for SM, in order to further increase its ADRs in point-

to-point closed-loop MIMO systems. Originally, the number of TAs in an SM system was assumed to be a power of two for the sake of convenient bit-to-TA mapping. To implement SM along with an arbitrary number of TAs, specific bit-padding [12] and modulation-varying [13] schemes have been proposed for offering flexible scalability. Later on, SM has been adopted in a wide range of applications, such as visible light communications [14], [15], physical-layer security [16], [17], and reconfigurable intelligent surfaces [18], [19].

In general, the SM is composed of space-shift keying (SSK) and amplitude/phase-shift keying (APSK). There are two bit-sequences: one is mapped onto the SSK symbols via TA selection, while the other is mapped onto the APSK symbols via classic modulation. An SSK symbol and an APSK symbol jointly form a group, where the latter is physically radiated from the TA activated by the former. Since the two bit-sequences are independent of each other, the radiation of an APSK-modulated symbol and the mapping onto an SSK-activated TA are two independent information processes in the SM.

Through linking up these two processes, we propose a new transmission scheme, referred to as difference-based spatial modulation (DBSM), for improving the SM performance via Euclidean distance maximisation. The DBSM consists of two steps: Firstly, all the information bits (without channel coding) or coded bits (with channel coding) to be transmitted are mapped onto APSK symbols, and two consecutive symbols form a group. Subsequently, the first APSK symbol in a group is physically radiated from the TA activated by the difference between the two symbols in the group. In contrast to the conventional SM, the DBSM selects the active TA based on the difference between two consecutive APSK symbols rather than solely upon an independent SSK symbol. For example, Fig. 1 compares the information mapping patterns of DBSM and conventional SM in a binary phase-shift keying (BPSK) system with 2 TAs. Each group contains two bits, and the first bit is mapped onto a BPSK symbol. Using the conventional SM, the second bit is mapped onto a SSK symbol, determining which TA is activated to transmit the BPSK symbol mapped by the first bit. Using our DBSM, *the active TA is determined by the difference between the two bits in a group*. If they are equal, TA 1 is activated. If they are different, TA 2 is activated. We remark that, the DBSM is fundamentally different from differential SM [20], [21]. The latter is designed for non-coherent detection dispensing with explicit channel estimation and its pilot overhead. However, the non-coherent detection performance is 3dB worse than that of the conventional SM with coherent detection. By contrast, the DBSM is specifically designed for improving the SM performance relying on coherent detection, whose resultant Euclidean distance is larger than that of conventional SM.

In essence, the DBSM allows the bits mapped onto the active TA and the bits carried by the radiated APSK symbol

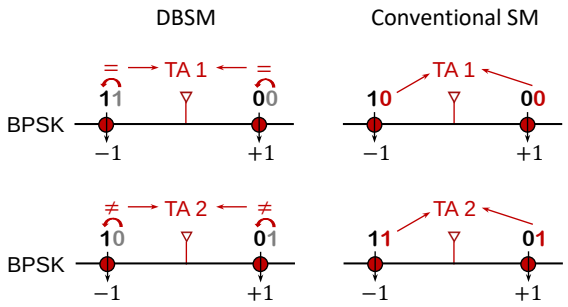

FIGURE 1. Comparison of information mapping patterns in DBSM and conventional SM.

to check each other. Although the second APSK symbol in a group is not physically radiated, the bits carried by it are conveyed not only through the selection of the active TA but also through the radiation of the first APSK symbol. As such, the DBSM enhances the detection performance by taking advantage of the transmission diversity over two types of physical resources.

As substantiated by the simulation results in [1], DBSM outperforms the conventional SM for low modulation orders, e.g., BPSK and quadrature phase-shift keying (QPSK). In this paper, both the throughput and the reliability of DBSM systems are analysed theoretically. In particular, the metrics of ADR and bit error rate (BER) are formulated in analytic expressions for the DBSM. Additionally, the BER performance of channel-coded DBSM systems is characterised.

The main contributions of this paper are highlighted below from four perspectives.

- *Approach:* A new multi-antenna transmission scheme, referred to as DBSM, is proposed for improving the reliability of SM systems, where the difference between two consecutive APSK symbols, rather than an independent SSK symbol, is mapped onto the active TA.
- *Rationale:* The design principle of the APSK constellation used in the DBSM is outlined to ensure that the mean Euclidean distance between any two DBSM-formed signals having the largest number of different bits is the largest among all the candidates, which is the key for DBSM to achieve higher reliability than conventional SM.
- *Throughput:* The ADR framework is established for the DBSM performance analysis in various system configurations, to create useful tools for information-theoretical investigations in the context of spectral efficiency and energy efficiency.
- *Reliability:* The BERs of DBSM are formulated by the expressions in analytic form, for various system configurations, to facilitate the empirical performance evaluation. The accuracy of BER expressions is explicitly confirmed by illustrative simulation results. Finally, the BERs of channel-coded DBSM systems are quantified.

TABLE 1. Contrasting the novelty of our work to the literature.

Contribution	This Work	[1]	[4]–[6]	[7]–[11]	[12]	[13]
Source-Difference-Based Mapping	✓	✓				
Spatial Modulation	✓	✓	✓	✓	✓	✓
Constellation Design	✓					
Data Rate	✓			✓	✓	
Bit Error Rate	✓	✓			✓	✓
Channel-Coded Systems	✓					

Furthermore, the novelty of our work is compared with related works in Table 1.

To detail the aforementioned contributions, the remainder of this paper is organised as follows. Section II presents the proposed DBSM in the context of MIMO systems and specifies the particular design principles of the APSK constellation constructed for the DBSM. Section III analyses the ADRs of the DBSM and compares the DBSM with the conventional SM from an information-theoretical perspective. Section IV investigates the BERs of both uncoded and channel-coded DBSM systems with various configurations, as well as compares them with those of the conventional SM in the same system configurations. Finally, Section V concludes the paper and offers insights for future research directions.

Throughout the paper, the acronyms listed in Table 2 and the following mathematical notations are used: boldface uppercase and lowercase letters denote matrices and vectors, respectively. In particular, $\mathbf{0}_{N\times 1}$ denotes the $N \times 1$ zero vector, and $\mathbf{I}_N$ represents the $N \times N$ identity matrix. The transpose, the conjugate transpose and the Frobenius norm of a vector or a matrix are denoted by $(\cdot)^{\mathrm{T}}$, $(\cdot)^{\dagger}$ and $\|\cdot\|$, respectively. Moreover, the modulus operator is represented by $|\cdot|$, and the expectation (mean) operator with respect to the random variable x is denoted by $\mathcal{E}_x\{\cdot\}$. The Q-function is given by $Q(x) = (1/\sqrt{2\pi})\int_x^{\infty} \exp(-u^2/2)du$. More specifically, the prime notations used in this paper are listed in Table 3.

TABLE 2. List of Acronyms

Acronym	Full Form
ADR	Achievable Data Rate
APSK	Amplitude/Phase-Shift Keying
AWGN	Additive White Gaussian Noise
BER	Bit Error Rate
BPSK	Binary Phase-Shift Keying
DBSM	Difference-Based Spatial Modulation
LLR	Log-Likelihood Ratio
MIMO	Multiple-Input-Multiple-Output
QAM	Quadrature Amplitude Modulation
QPSK	Quadrature Phase-Shift Keying
RA	Receive Antenna
RF	Radio Frequency
SM	Spatial Modulation
SNR	Signal-to-Noise power Ratio
SSK	Space-Shift Keying
TA	Transmit Antenna
V-BLAST	Vertical Bell Laboratories Layered Space-Time

II. DIFFERENCE-BASED SPATIAL MODULATION

In this section, the DBSM concept is proposed for MIMO systems and a BPSK-modulated paradigm is presented to illustrate the DBSM design. Furthermore, the particular design principle of the APSK constellation constructed for DBSM is described.

A. SYSTEM MODEL

Consider a point-to-point (M, N) MIMO communication system having M TAs and N receive antennas (RAs). The flat-fading narrow-band channel, spanning from the transmitter to the receiver, is modelled by an $N \times M$ matrix

$$\mathbf{H} = \begin{bmatrix} h_{11} & h_{12} & \cdots & h_{1M} \\ h_{21} & h_{22} & \cdots & h_{2M} \\ \vdots & \vdots & \ddots & \vdots \\ h_{N1} & h_{N2} & \cdots & h_{NM} \end{bmatrix}, \tag{1}$$

where the $(n, m)^{\mathrm{th}}$ entry, denoted by h_{nm}, is the channel coefficient of the link from TA m to RA n, with $m \in \{1, 2, \cdots, M\}$ and $n \in \{1, 2, \cdots, N\}$. The entries are assumed to be independent and identically distributed

TABLE 3. List of Prime Notations.

Notation	Description
(M, N)	a system with M TAs and N RAs
$\mathbf{h}_m$	the channel from TA m to the receiver
$\mathbf{y}$	a vector containing received signals
$\mathbf{z}$	a vector containing received noise
Θ_k or Θ_l	an MQAM symbol
$d = (l-k) \bmod M$	the index difference of two MQAM symbols

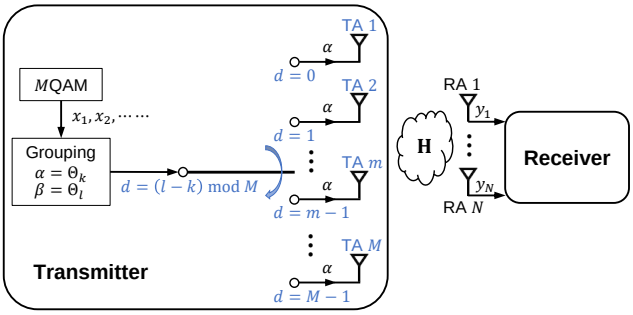

FIGURE 2. The DBSM with MQAM in an (M, N) system.

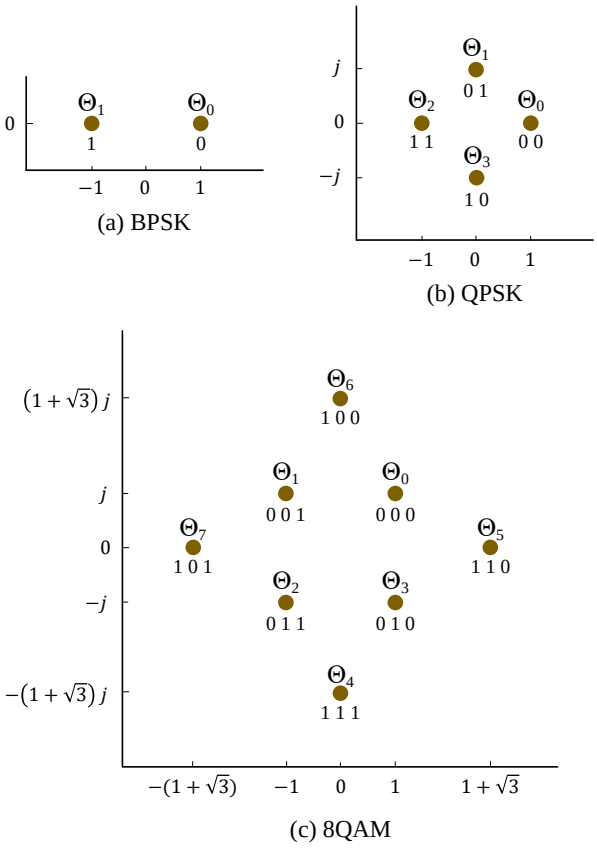

FIGURE 3. BPSK, QPSK and 8QAM constellations in the DBSM.

(i.i.d.) complex Gaussian random variables with zero-mean and unit variance, i.e., we have $h_{nm} \sim \mathcal{CN}(0, 1)$. The m^{th} column in (1), denoted by an $N \times 1$ vector $\mathbf{h}_m = [h_{1m}, h_{2m}, \cdots, h_{Nm}]^{\text{T}}$, contains the channel coefficients of the links from TA m to all the RAs, $m = 1, 2, \cdots, M$.

The DBSM within an (M, N) system is shown in Fig. 2, where M-ary quadrature amplitude modulation (MQAM) is adopted. The i^{th} modulated symbol, $i = 1, 2, \cdots$, is denoted by $x_i \in \{\Theta_0, \Theta_1, \cdots, \Theta_{M-1}\}$, where Θ_k is the k^{th} symbol in the MQAM constellation, $k \in \{0, 1, \cdots, M-1\}$. For example, the indexing and mapping of the symbols in BPSK, QPSK, and 8QAM constellations are shown in Fig. 3.

With DBSM, a pair of modulated symbols are delivered simultaneously in each channel-use. More specifically, the two modulated symbols to be delivered in the p^{th} transmission, $p = 1, 2, \cdots$, are denoted by $\alpha = x_{2p-1}$ and $\beta = x_{2p}$. Without loss of generality, we set $\alpha = \Theta_k$ and $\beta = \Theta_l$, $k, l \in \{0, 1, \cdots, M-1\}$.

In the transmission, β is not physically radiated, while α is radiated from one of the TAs. The active TA is determined by the difference between β and α, which is informed by the difference between the indices of the MQAM symbols Θ_k and Θ_l, expressed as

$$d = (l-k) \bmod M. \tag{2}$$

Elaborating slightly further, α is radiated from TA $(d+1)$. For instance, TA 1 is activated when $d = 0$, i.e., $\beta = \alpha$, and TA 2 is activated when $d = 1$, i.e., $\beta = \Theta_{k+1}$ whilst $\alpha = \Theta_k$.

The received signals are contained by an $N \times 1$ vector expressed as

$$\mathbf{y} = \mathbf{h}_{d+1}\alpha + \mathbf{z}, \tag{3}$$

where $\mathbf{y} = [y_1, y_2, \cdots, y_N]^{\text{T}}$ with y_n denoting the received signal at RA n, and the $N \times 1$ vector $\mathbf{z} = [z_1, z_2, \cdots, z_N]^{\text{T}}$ contains i.i.d. additive white Gaussian noise (AWGN) components at the receiver, with $z_n \sim \mathcal{CN}(0, \sigma_Z^2)$ denoting the AWGN component received by the n^{th} RA, $n = 1, 2, \cdots, N$. Moreover, the $N \times 1$ vector $\mathbf{h}_{d+1}$ represents the channel spanning from the active TA, namely TA $(d+1)$, to the receiver, with d given in (2).

The task of detection is to find not only the radiated symbol α but also the activated channel $\mathbf{h}_{d+1}$. Apparently, the maximum likelihood (ML) detection algorithm can be used for estimating the symbols α and β simultaneously as follows. Choose $\hat{\alpha} = \Theta_k$ and $\hat{\beta} = \Theta_{(m-1+k) \bmod M}$ if and only if

$$\begin{aligned} \|\mathbf{y} - \mathbf{h}_m\Theta_k\|^2 \leqslant \|\mathbf{y} - \mathbf{h}_{m'}\Theta_{k'}\|^2, \\ \forall m, m' = 1, 2, \cdots, M, \quad m \neq m', \\ k, k' = 0, 1, \cdots, M-1, \quad k \neq k'. \end{aligned} \tag{4}$$

To reduce the computational complexity, the ML detection in (4) can be partitioned into two steps: Firstly, the candidate decisions are made concerning the symbol radiated from TA

TABLE 4. Computational Complexity.

ML Detection	# Multiplications	# Comparisons
(4)	M^2	M^2-1
(5)-(6)	$2M$	$2M-1$

m, denoted by $\hat{\alpha}_m$, in terms of

$$\hat{\alpha}_m = \arg \min_{s\in\{\Theta_0,\Theta_1,\cdots,\Theta_{M-1}\}} \left| s - \frac{\mathbf{h}_m^\dagger \mathbf{y}}{\mathbf{h}_m^\dagger \mathbf{h}_m} \right|^2, \quad m = 1,2,\cdots,M; \tag{5}$$

and then, choose $\hat{\alpha} = \hat{\alpha}_{\hat{m}}$ and $\hat{\beta} = \Theta_{(\hat{m}-1+\sharp\hat{\alpha}) \bmod M}$ if and only if

$$\hat{m} = \arg \min_{m\in\{1,2,\cdots,M\}} \|\mathbf{y} - \mathbf{h}_m \hat{\alpha}_m\|^2, \tag{6}$$

where $\sharp\hat{\alpha} = k \in \{0,1,\cdots,M-1\}$ denotes the index of the symbol $\hat{\alpha}$, given that $\hat{\alpha} = \Theta_k$.

The computational complexities of both the ML detection (4) and the two-step ML detection (5)-(6) are characterised in Table 4, where the detection complexity is quantified in terms of the number of multiplications and the number of comparisons. These two ML algorithms achieve the same performance. However, the complexity of the two-step detection (5)-(6) is lower than that of the detection (4), especially for high M.

Moreover, the detection complexity of the DBSM is the same as that of the conventional SM in the same system configuration [7], for both the ML algorithm (4) and the two-step ML algorithm (5)-(6).

B. A PARADIGM

Herein, a BPSK-modulated $(2, N)$ system is considered as an example to further elucidate the DBSM design. There are $M = 2$ columns in the channel matrix, i.e., we have $\mathbf{H} = [\mathbf{h}_1, \mathbf{h}_2]$, where the $N \times 1$ vectors $\mathbf{h}_1$ and $\mathbf{h}_2$ contain the channel coefficients of the links spanning from TA 1 and TA 2 to the receiver, respectively.

The DBSM paradigm is illustrated in Fig. 4, where the modulated symbols are generated through the BPSK constellation shown in Fig. 3(a), i.e., $x_i \in \{+1,-1\}$, $i = 1,2,\cdots$. For a group composed of two symbols α and β, we might have either $\beta = \alpha$ or $\beta = -\alpha$. Therefore, in an DBSM transmission, α is radiated from TA 1 if $\beta = \alpha$, and from TA 2 if $\beta = -\alpha$. Thus, the index of the active TA is denoted by

$$\sharp(\beta = \pm\alpha) = \begin{cases} 1, & \text{if } \beta = \alpha; \\ 2, & \text{if } \beta = -\alpha. \end{cases} \tag{7}$$

As such, the received signals are contained by an $N \times 1$ vector expressed as

$$\mathbf{y} = \mathbf{h}_{\sharp(\beta=\pm\alpha)}\alpha + \mathbf{z}, \tag{8}$$

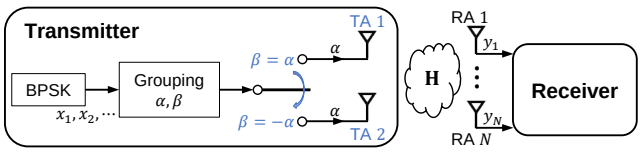

FIGURE 4. The DBSM in a BPSK-modulated system.

where the $N \times 1$ vector $\mathbf{h}_{\sharp(\beta=\pm\alpha)}$ denotes the channel spanning from the active TA to the receiver.

Using the ML detection algorithm, the estimates of the symbols α and β can be simultaneously obtained from

$$\mathbb{E} = \min\{\|\mathbf{y} - \mathbf{h}_1\|^2, \|\mathbf{y} + \mathbf{h}_1\|^2, \|\mathbf{y} - \mathbf{h}_2\|^2, \|\mathbf{y} + \mathbf{h}_2\|^2\}. \tag{9}$$

In detail, the estimation is formulated as

$$\begin{cases} \hat{\alpha} = \hat{\beta} = +1, & \text{if } \mathbb{E} = \|\mathbf{y} - \mathbf{h}_1\|^2; \\ \hat{\alpha} = \hat{\beta} = -1, & \text{if } \mathbb{E} = \|\mathbf{y} + \mathbf{h}_1\|^2; \\ \hat{\alpha} = +1, \hat{\beta} = -1, & \text{if } \mathbb{E} = \|\mathbf{y} - \mathbf{h}_2\|^2; \\ \hat{\alpha} = -1, \hat{\beta} = +1, & \text{if } \mathbb{E} = \|\mathbf{y} + \mathbf{h}_2\|^2. \end{cases} \tag{10}$$

Note that, as $M = 2$ in this paradigm, the detection complexity using (4) is the same as that using the two-step ML of (5)-(6).

C. DESIGN PRINCIPLE

The key for the DBSM to improve the reliability of SM systems is the MQAM constellation design, specifically for higher-order APSK modulations. In particular, every MQAM symbol Θ_k has to be appropriately indexed by $k \in \{0,1,\cdots,M-1\}$ and mapped by the bit-sequence $b_1 b_2 \cdots b_U$, where $U = \log_2 M$ and $b_u \in \{0,1\}$ denotes a bit in the sequence, $u \in \{1,2,\cdots,U\}$.

The main objective of the indexing $k \in \{0,1,\cdots,M-1\}$ and the mapping $b_1 b_2 \cdots b_U \leftrightarrow \Theta_k$ is to ensure that the mean Euclidean distance between any two DBSM signals mapped by the complementary bit-sequences of length $2\log_2 M$ is the largest possible among all the candidates.

1) BPSK-Modulated DBSM

Based on Fig. 3(a) and (10), all the DBSM-formed signals in a BPSK-modulated system associated with $M = 2$ are listed in Table 5, where the conventional SM-formed signals in the same system configuration are presented as well for the sake of comparison. Subsequently, every Euclidean distance between two DBSM signals with $M = 2$ is compared to that between two conventional SM signals with the same system configuration in Table 6, where each shaded cell contains the Euclidean distance between a pair of DBSM signals mapped by two complementary bit-sequences of length $2\log_2 M = 2$, i.e., the number of different bits in these two bit-sequences is 2. In this case, the DBSM has the Euclidean distance $\|2\mathbf{h}_m\|$ along with $2\mathbf{h}_m \sim \mathcal{CN}(\mathbf{0}_{N\times 1}, 4\mathbf{I}_N)$, $m = 1,2$, whilst the conventional SM has the Euclidean distance

TABLE 5. DBSM/SM-Formed Signals in the Systems with $M = 2$.

	DBSM	Conventional SM
00	$\mathbf{h}_1$	$\mathbf{h}_1$
01	$\mathbf{h}_2$	$\mathbf{h}_2$
10	$-\mathbf{h}_2$	$-\mathbf{h}_1$
11	$-\mathbf{h}_1$	$-\mathbf{h}_2$

TABLE 6. Euclidean Distances in the Systems with $M = 2$.

DBSM

	00	01	10	11
00	0	$\|\mathbf{h}_1 - \mathbf{h}_2\|$	$\|\mathbf{h}_1 + \mathbf{h}_2\|$	$\|2\mathbf{h}_1\|$
01	$\|\mathbf{h}_1 - \mathbf{h}_2\|$	0	$\|2\mathbf{h}_2\|$	$\|\mathbf{h}_1 + \mathbf{h}_2\|$
10	$\|\mathbf{h}_1 + \mathbf{h}_2\|$	$\|2\mathbf{h}_2\|$	0	$\|\mathbf{h}_1 - \mathbf{h}_2\|$
11	$\|2\mathbf{h}_1\|$	$\|\mathbf{h}_1 + \mathbf{h}_2\|$	$\|\mathbf{h}_1 - \mathbf{h}_2\|$	0

Conventional SM

	00	01	10	11
00	0	$\|\mathbf{h}_1 - \mathbf{h}_2\|$	$\|2\mathbf{h}_1\|$	$\|\mathbf{h}_1 + \mathbf{h}_2\|$
01	$\|\mathbf{h}_1 - \mathbf{h}_2\|$	0	$\|\mathbf{h}_1 + \mathbf{h}_2\|$	$\|2\mathbf{h}_2\|$
10	$\|2\mathbf{h}_1\|$	$\|\mathbf{h}_1 + \mathbf{h}_2\|$	0	$\|\mathbf{h}_1 - \mathbf{h}_2\|$
11	$\|\mathbf{h}_1 + \mathbf{h}_2\|$	$\|2\mathbf{h}_2\|$	$\|\mathbf{h}_1 - \mathbf{h}_2\|$	0

$\|\mathbf{h}_1 + \mathbf{h}_2\|$ with $\mathbf{h}_1 + \mathbf{h}_2 \sim \mathcal{CN}(\mathbf{0}_{N\times 1}, 2\mathbf{I}_N)$. That is, the mean of the squared Euclidean distance using the DBSM is twice that using the conventional SM in this case, i.e., we have $\mathcal{E}\{\|2\mathbf{h}_m\|^2\} = 2\mathcal{E}\{\|\mathbf{h}_1 + \mathbf{h}_2\|^2\}$. More specifically, the BPSK-modulated DBSM guarantees that the largest mean Euclidean distance $\mathcal{E}\{\|2\mathbf{h}_m\|\}$, $m \in \{1, 2\}$, between two DBSM signals is imposed on a pair of bit-sequences having the largest number of different bits.

2) QPSK-Modulated DBSM

Based on Fig. 3(b) and (4), all the DBSM signals of a QPSK-modulated system associated with $M = 4$ are listed in Table 7, along with the conventional SM signals using the same system configuration, where the two bit-sequences of length $2\log_2 M = 4$ in each row are the complements of each other, i.e., they have 4 different bits. Obviously, the Euclidean distance between the two DBSM signals in each row is $\|2\mathbf{h}_m\|$, and the Euclidean distance between the two

TABLE 7. DBSM/SM-Formed Signals in the Systems with $M = 4$.

	DBSM	SM		DBSM	SM
0000	$\mathbf{h}_1$	$\mathbf{h}_1$	1111	$-\mathbf{h}_1$	$-\mathbf{h}_3$
0001	$\mathbf{h}_2$	$\mathbf{h}_2$	1110	$-\mathbf{h}_2$	$-\mathbf{h}_4$
0011	$\mathbf{h}_3$	$\mathbf{h}_3$	1100	$-\mathbf{h}_3$	$-\mathbf{h}_1$
0010	$\mathbf{h}_4$	$\mathbf{h}_4$	1101	$-\mathbf{h}_4$	$-\mathbf{h}_2$
0100	$j\mathbf{h}_4$	$j\mathbf{h}_1$	1011	$-j\mathbf{h}_4$	$-j\mathbf{h}_3$
0101	$j\mathbf{h}_1$	$j\mathbf{h}_2$	1010	$-j\mathbf{h}_1$	$-j\mathbf{h}_4$
0111	$j\mathbf{h}_2$	$j\mathbf{h}_3$	1000	$-j\mathbf{h}_2$	$-j\mathbf{h}_1$
0110	$j\mathbf{h}_3$	$j\mathbf{h}_4$	1001	$-j\mathbf{h}_3$	$-j\mathbf{h}_2$

conventional SM signals in each row is $\|\mathbf{h}_m + \mathbf{h}_{m'}\|$, where $m, m' = 1, 2, 3, 4$ and $|m - m'| = 2$. As such, the largest mean Euclidean distance $\mathcal{E}\{\|2\mathbf{h}_m\|\}$, $m \in \{1, 2, 3, 4\}$, is guaranteed by the QPSK-modulated DBSM for any two DBSM signals mapped by the two bit-sequences that have the largest number of different bits, namely $2\log_2 M = 4$.

3) 8QAM-Modulated DBSM

Based on Fig. 3(c) and (4) with $M = 8$, the Euclidean distance between any two DBSM signals mapped by the complementary bit-sequences of length $2\log_2 M = 6$ is $\|\sqrt{8 + 4\sqrt{3}}\mathbf{h}_m\|$, $m \in \{1, 2, \cdots, 8\}$. As the average energy per 8QAM symbol in Fig. 3(c) is $3 + \sqrt{3}$, the normalised Euclidean distance applied to the two bit-sequences having the largest number of different bits is $\|\sqrt{2 + 2/\sqrt{3}}\mathbf{h}_m\|$.

4) Generalised Criteria

For an MQAM-modulated DBSM system, the MQAM constellation design meets the following criteria.

- For the *indexing*, the index difference between the two MQAM symbols mapped by a pair of complementary bit-sequences having length $U = \log_2 M$ is $M/2$, i.e., $|k - k'| = M/2$ given that $b_1 b_2 \cdots b_U \leftrightarrow \Theta_k$ and $\bar{b}_1 \bar{b}_2 \cdots \bar{b}_U \leftrightarrow \Theta_{k'}$, where $\bar{b}_u$ is the complement of b_u, $u = 1, 2, \cdots, U$. This criterion guarantees that the same TA, i.e., the same channel state $\mathbf{h}_m$, $m \in \{1, 2, \cdots, M\}$, will be activated in the two DBSM signals that are mapped by complementary bit-sequences of length $2\log_2 M$.
- For the *mapping*, any pair of complementary bit-sequences having length $U = \log_2 M$, i.e., $b_1 b_2 \cdots b_U$ and $\bar{b}_1 \bar{b}_2 \cdots \bar{b}_U$, are mapped onto the two specific MQAM symbols that have the same largest possible Euclidean distance δ. In other words, the same δ is applied to each pair of MQAM symbols mapped by complementary bit-sequences. This criterion further

$$R_{\mathrm{DB}} = \log_2(M^2) - \frac{1}{M^2}\sum_{k=0}^{M-1}\sum_{l=0}^{M-1}\mathcal{E}_{\mathbf{z}}\Bigg\{\log_2\Bigg(\underbrace{1+\sum_{\substack{k'=0\\(k',l')\neq(k,l)}}^{M-1}\sum_{l'=0}^{M-1}\exp\Big(-\rho\big(\|\mathbf{d}_{l,l'}^{k,k'}+\mathbf{z}\|^2-\|\mathbf{z}\|^2\big)\Big)}_{f_{\mathrm{DB}}(\rho)}\Bigg)\Bigg\} \tag{13}$$

constructs $\|\delta\mathbf{h}_m\|$ as the Euclidean distance between any two DBSM signals mapped by the complementary bit-sequences of length $2\log_2 M$.

The indexing and mapping criteria ensure that any pair of complementary bit-sequences having length $2\log_2 M$ are eventually mapped onto the two DBSM signals that have the largest mean Euclidean distance, thus leading to the DBSM having higher reliability than the conventional SM. The detailed reason behind this will be further clarified using the BER performance analysis in Section IV-A.

III. ACHIEVABLE DATA RATE

To evaluate the spectral efficiency and the spatial multiplexing gain achieved by the proposed DBSM, the analysis framework of its ADRs is established in the discrete-input continuous-output memoryless channel model, for various system configurations. Moreover, the ADRs of the conventional SM are presented within the same system configurations for the sake of comparison.

Based on (3), the received signals of an (M,N) DBSM system can be rewritten as

$$\mathbf{y} = \mathbf{H}\mathbf{W}\begin{bmatrix}\alpha\\ \beta\end{bmatrix} + \mathbf{z} = \mathbf{H}\mathbf{W}\begin{bmatrix}\Theta_k\\ \Theta_l\end{bmatrix} + \mathbf{z}, \qquad k,l \in \{0,1,\cdots,M-1\}, \tag{11}$$

where

$$\mathbf{W} = \frac{1}{2}\begin{bmatrix}1 & -\Theta_k/\Theta_l\\ \vdots & \vdots\\ 1 & -\Theta_k/\Theta_l\\ 1 & \Theta_k/\Theta_l\\ 1 & -\Theta_k/\Theta_l\\ \vdots & \vdots\\ 1 & -\Theta_k/\Theta_l\end{bmatrix}\begin{matrix}\Big\}(l-k) \bmod M\\ \\ \Big\}(M-1)-((l-k) \bmod M)\end{matrix} \tag{12}$$

is an $M\times 2$ matrix carrying out the DBSM.

To keep consistency in the expression, the AWGN power at the receiver is denoted by σ_Z^2, and the normalised signal-to-noise power ratio (SNR) is denoted by $\rho = 1/\sigma_Z^2$, where the average energy per transmitted MQAM symbol is normalised to unity.

Given a realisation of the channel matrix $\mathbf{H}$, the instantaneous ADR of the DBSM using MQAM in an (M,N) system is formulated by (13), where the $N\times 1$ vector

$$\mathbf{d}_{l,l'}^{k,k'} = \mathbf{H}\left(\mathbf{W}\begin{bmatrix}\Theta_k\\ \Theta_l\end{bmatrix} - \mathbf{W}'\begin{bmatrix}\Theta_{k'}\\ \Theta_{l'}\end{bmatrix}\right) \tag{14}$$

is associated with $k,k',l,l' \in \{0,1,\cdots,M-1\}$, and $(k',l')\neq(k,l)$ excludes the event when $k'=k$ and $l'=l$ simultaneously occur from the summation, as $\mathbf{d}_{l,l'}^{k,k'} = \mathbf{0}_{N\times 1}$ and $\exp(-\rho(\|\mathbf{d}_{l,l'}^{k,k'}+\mathbf{z}\|^2-\|\mathbf{z}\|^2)) = 1$ in the case that $k'=k$ and $l'=l$ simultaneously occur. The $M\times 2$ matrix $\mathbf{W}$ is given by (12), and

$$\mathbf{W}' = \frac{1}{2}\begin{bmatrix}1 & -\Theta_{k'}/\Theta_{l'}\\ \vdots & \vdots\\ 1 & -\Theta_{k'}/\Theta_{l'}\\ 1 & \Theta_{k'}/\Theta_{l'}\\ 1 & -\Theta_{k'}/\Theta_{l'}\\ \vdots & \vdots\\ 1 & -\Theta_{k'}/\Theta_{l'}\end{bmatrix}\begin{matrix}\Big\}(l'-k') \bmod M\\ \\ \Big\}(M-1)-((l'-k') \bmod M)\end{matrix}$$

is the $M\times 2$ matrix to carry out the DBSM for the symbols $\Theta_{k'}$ and $\Theta_{l'}$.

By contrast, the instantaneous ADR of conventional SM using MQAM in an (M,N) system is expressed as (15), where the $N\times 1$ vector

$$\mathbf{q}_{m,m'}^{k,k'} = \mathbf{h}_m\Theta_k - \mathbf{h}_{m'}\Theta_{k'} \tag{16}$$

is associated with $m,m' \in \{1,2,\cdots,M\}$ and $k,k' \in \{0,1,\cdots,M-1\}$, excluding the event when $m'=m$ and $k'=k$ occur together from the summation.

For a given channel realisation, $f_{\mathrm{DB}}(\rho)$ in (13) and $f_{\mathrm{SM}}(\rho)$ in (15) are both monotonically decreasing functions of the normalised SNR ρ, and both of them converge to 1, when ρ tends to infinity, i.e.,

$$\lim_{\rho\to+\infty} f_{\mathrm{DB}}(\rho) = \lim_{\rho\to+\infty} f_{\mathrm{SM}}(\rho) = 1. \tag{17}$$

Thus, as ρ approaches infinity, we have the limit

$$\lim_{\rho\to+\infty} R_{\mathrm{DB}}(\rho) = \lim_{\rho\to+\infty} R_{\mathrm{SM}}(\rho) = \log_2(M^2), \tag{18}$$

which is the upper bound on the ADRs of both DBSM and conventional SM, using MQAM in an (M,N) system.

In Fig. 5, the ergodic ADR of the DBSM, i.e., $\mathcal{E}_{\mathbf{H}}\{R_{\mathrm{DB}}\}$, is compared with that of the conventional SM, i.e., $\mathcal{E}_{\mathbf{H}}\{R_{\mathrm{SM}}\}$, for various system configurations using the constellations given in Fig. 3. As shown in Fig. 5, the DBSM achieves the same ergodic ADR as the conventional SM, i.e., $\mathcal{E}_{\mathbf{H}}\{R_{\mathrm{DB}}\} = \mathcal{E}_{\mathbf{H}}\{R_{\mathrm{SM}}\}$, in the same system configuration. The reason behind this is that the varied forms of $\mathbf{d}_{l,l'}^{k,k'}$ in (14) with $k,k',l,l' = 0,1,\cdots,M-1$ are the same as those of $\mathbf{q}_{m,m'}^{k,k'}$ in (16) with $m,m' = 1,2,\cdots,M$, $k,k' = 0,1,\cdots,M-1$ and, moreover, all the varied forms occur at the same probability, which leads to the same ergodic values of (13) and (15).

$$R_{\mathrm{SM}} = \log_2(M^2) - \frac{1}{M^2}\sum_{m=1}^{M}\sum_{k=0}^{M-1}\mathcal{E}_{\mathbf{z}}\left\{\log_2\left(1+\underbrace{\sum_{\substack{m'=1\\(m',k')\neq(m,k)}}^{M}\sum_{k'=0}^{M-1}\exp\left(-\rho\left(\|\mathbf{q}_{m,m'}^{k,k'}+\mathbf{z}\|^2-\|\mathbf{z}\|^2\right)\right)}_{f_{\mathrm{SM}}(\rho)}\right)\right\} \tag{15}$$

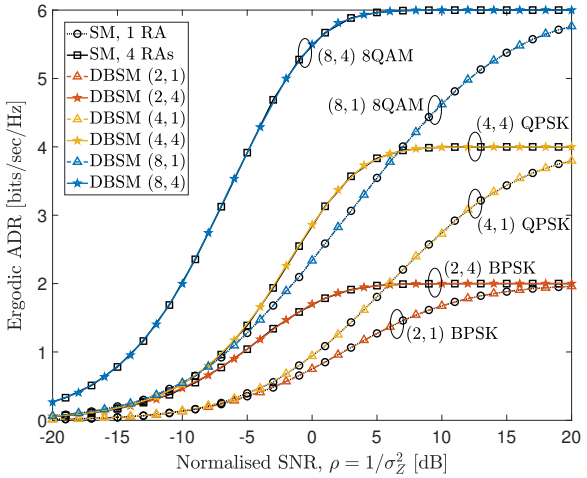

FIGURE 5. Ergodic ADR comparisons between DBSM and conventional SM for various system configuration.

As the normalised SNR ρ increases, i.e., as the AWGN power σ_Z^2 decreases, the ergodic ADRs of both the DBSM and the conventional SM converge to the same value, namely $2\log_2 M$ bits/sec/Hz, which agrees with the limit given in (18). Since this limit is not affected by the number of RAs, N, the ergodic ADR of an DBSM or SM system associated with any number of RAs converges to the same value, as exemplified by comparing the cases of $N = 1$ and $N = 4$ in Fig. 5.

In addition, the ADRs of the DBSM with $M = 2$ converge faster than those of the DBSM with $M > 2$. The main reason behind this is that the DBSM with $M = 2$ achieves higher spatial multiplexing gain than the DBSM with $M > 2$. The spatial multiplexing gain of a MIMO system having Gaussian-distributed inputs is defined in [22, Eq. (3)] as

$$\lim_{\rho\to\infty}\frac{C(\rho)}{\log_2\rho}, \tag{19}$$

where $C(\rho)$ is the error-free channel capacity and $\log_2\rho$ is the amount of bits carried by a signal, as the SNR ρ tends to infinity. However, the definition (19) cannot be directly applied to a MIMO system having finite-alphabet modulations, since the ADR $R(\rho)$ converges to a constant and the ratio $R(\rho)/\log_2\rho$ approaches zero as ρ goes to infinity.

As such, the spatial multiplexing gain of a MIMO system with finite-alphabet modulations can be characterised as the ADR normalised with respect to the received SNR [22]. The instantaneous SNR at the DBSM receiver can be expressed as

$$\rho\mathbf{H}\mathbf{W}\mathbf{R}_X\mathbf{W}^\dagger\mathbf{H}^\dagger = \rho\mathbf{H}\mathbf{W}\mathbf{W}^\dagger\mathbf{H}^\dagger \triangleq \rho\tilde{\mathbf{H}}\tilde{\mathbf{H}}^\dagger, \tag{20}$$

where $\mathbf{R}_X = \mathbf{I}_2$ is the covariance matrix of the two MQAM symbols $[\alpha,\beta]^{\mathrm{T}}$ in an arbitrary transmission. Note that, in an DBSM system with $M = 2$, i.e., using BPSK modulation and two TAs, the matrix $\mathbf{W}$ in (12) is always

$$\frac{1}{2}\begin{bmatrix}1 & 1\\ 1 & -1\end{bmatrix}. \tag{21}$$

Thus, we have $\mathbf{W}\mathbf{W}^\dagger = (1/2)\mathbf{I}_2$ and $\tilde{\mathbf{H}}\tilde{\mathbf{H}}^\dagger = (1/2)\mathbf{H}\mathbf{H}^\dagger$ in (20) for the DBSM with $M = 2$.

In particular, the received SNR of the vertical Bell Laboratories layered space-time architecture (V-BLAST) is $\rho\mathbf{H}\mathbf{H}^\dagger$ [23], and the received SNR of the DBSM with $M = 2$ is $\rho\tilde{\mathbf{H}}\tilde{\mathbf{H}}^\dagger = (1/2)\rho\mathbf{H}\mathbf{H}^\dagger$. This indicates that the spatial multiplexing gain of the DBSM with $M = 2$ is equivalent to that of the V-BLAST, which is the full spatial multiplexing gain achieved by a MIMO system [22].

On the other hand, the received SNR of the DBSM with $M = 2$ is 3dB lower than that of the V-BLAST in the same system configuration. As observed from (11), the 3dB loss is incurred because the total radiated power of a single transmission in the DBSM system with $M = 2$ is half that of a single transmission in the V-BLAST system with the same configuration. In other words, if the total radiated power in a single transmission is kept identical for both the DBSM and the V-BLAST, i.e., by increasing the factor $1/2$ in the matrix (21) to $1/\sqrt{2}$, the DBSM with $M = 2$ will achieve the same received SNR as the V-BLAST with the same system configuration, i.e., $\rho\tilde{\mathbf{H}}\tilde{\mathbf{H}}^\dagger = \rho\mathbf{H}\mathbf{H}^\dagger$.

As M increases, namely $M > 2$, the product $\mathbf{W}\mathbf{W}^\dagger$ is formed as

$$\frac{1}{4}\begin{bmatrix}1+\theta^2 & \cdots & 1+\theta^2 & 1-\theta^2 & 1+\theta^2 & \cdots & 1+\theta^2\\ \vdots & \ddots & \vdots & \vdots & \vdots & \ddots & \vdots\\ 1+\theta^2 & \cdots & 1+\theta^2 & 1-\theta^2 & 1+\theta^2 & \cdots & 1+\theta^2\\ 1-\theta^2 & \cdots & 1-\theta^2 & 1+\theta^2 & 1-\theta^2 & \cdots & 1-\theta^2\\ 1+\theta^2 & \cdots & 1+\theta^2 & 1-\theta^2 & 1+\theta^2 & \cdots & 1+\theta^2\\ \vdots & \ddots & \vdots & \vdots & \vdots & \ddots & \vdots\\ 1+\theta^2 & \cdots & 1+\theta^2 & 1-\theta^2 & 1+\theta^2 & \cdots & 1+\theta^2\end{bmatrix},$$

where $\theta = \Theta_k/\Theta_l$. More specifically, all the entries in the $([(l-k)\bmod M]+1)^{\mathrm{th}}$ row and the $([(l-k)\bmod M]+1)^{\mathrm{th}}$ column, except for the $([(l-k)\bmod M]+1, [(l-k)\bmod M]+1)^{\mathrm{th}}$ entry, are $1-\theta^2$, whilst all the other entries are $1+\theta^2$. This matrix generates correlated rows and correlated columns in the product $\tilde{\mathbf{H}}\tilde{\mathbf{H}}^\dagger = \mathbf{H}\mathbf{W}\mathbf{W}^\dagger\mathbf{H}^\dagger$, thus reducing the spatial multiplexing gain.

IV. BIT ERROR RATE

From a mathematical perspective, the spatial diversity gain of a MIMO system is essentially obtained from the chi-squared distribution formed by multiple i.i.d. complex Gaussian random variables. Equivalently, the spatial diversity gain obtained by our DBSM is from the largest possible Euclidean distance, as shown in Section II-C.

The spatial multiplexing gain of a MIMO system is reflected by its ergodic ADR, and the spatial diversity gain of a MIMO system is reflected by its BER [22]. The ADRs of the DBSM associated with various system configurations have been analysed in Section III, illustrating the throughput and the spatial multiplexing gain achieved by the DBSM. In this section, the BERs of the DBSM are investigated to explicitly demonstrate its reliability while indicating the spatial diversity gain achieved by the largest possible Euclidean distance design.

To begin with, the BERs of the DBSM without channel coding in various system configurations are analysed for evaluating its stand-alone reliability and the performance gain achieved by itself over conventional SM. Then, the BERs of channel-coded DBSM systems are presented and compared with those of the channel-coded conventional-SM systems, to confirm that channel coding techniques will further enhance the performance gain achieved by the DBSM over conventional SM.

A. UNCODED SYSTEMS

As shown in (4), the ML algorithm is exploited for the detection of our DBSM. Given a realisation of the channel matrix $\mathbf{H}$, the BER of the DBSM is upper-bounded by the sum of pairwise error probabilities [24], expressed as

$$\epsilon_{\mathrm{DB}} = \frac{1}{M^2} \sum_{k=0}^{M-1} \sum_{l=0}^{M-1} \sum_{\substack{k'=0 \\ (k',l') \neq (k,l)}}^{M-1} \sum_{l'=0}^{M-1} \frac{N_{l \to l'}^{k \to k'}}{2 \log_2 M} Q\left(\frac{\| \mathbf{d}_{l,l'}^{k,k'} \|}{\sqrt{2\sigma_Z^2}} \right), \tag{22}$$

where the $N \times 1$ vector $\mathbf{d}_{l,l'}^{k,k'}$ is given in (14), and $N_{l \to l'}^{k \to k'}$ denotes the number of bits in error, when the vector $[\Theta_k, \Theta_l]^{\mathrm{T}}$ is mistaken for $[\Theta_{k'}, \Theta_{l'}]^{\mathrm{T}}$ by the ML detector, i.e., the number of different bits between these two pieces of information, $k, k', l, l' \in \{0, 1, \cdots, M-1\}$.

By contrast, the BER of the conventional SM using ML detection is upper-bounded by

$$\epsilon_{\mathrm{SM}} = \frac{1}{M^2} \sum_{m=1}^{M} \sum_{k=0}^{M-1} \sum_{\substack{m'=1 \\ (m',k') \neq (m,k)}}^{M} \sum_{k'=0}^{M-1} \frac{N_{m \to m'}^{k \to k'}}{2 \log_2 M} Q\left(\frac{\| \mathbf{q}_{m,m'}^{k,k'} \|}{\sqrt{2\sigma_Z^2}} \right), \tag{23}$$

where the $N \times 1$ vector $\mathbf{q}_{m,m'}^{k,k'}$ is given in (16), and $N_{m \to m'}^{k \to k'}$ denotes the number of bits in error when the vector $\mathbf{h}_m \Theta_k$ is mistaken for $\mathbf{h}_{m'} \Theta_{k'}$ by the ML detector, i.e., the number of different bits between these two pieces of information, $m, m' \in \{1, 2, \cdots, M\}$, $k, k' \in \{0, 1, \cdots, M-1\}$.

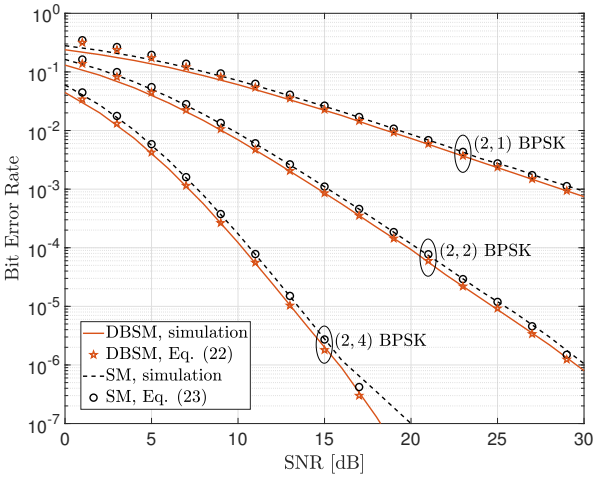

FIGURE 6. BER comparisons between DBSM and conventional SM in BPSK-modulated $(2, 1)$, $(2, 2)$, and $(2, 4)$ systems.

To illustrate the accuracy of the upper-bounds (22) and (23), Fig. 6 compares the BERs of the DBSM and the conventional SM in BPSK-modulated $(2, 1)$, $(2, 2)$, and $(2, 4)$ systems, where the numerical results based upon (22) and (23) are presented along with the simulation results. As shown in this figure, the upper-bounds are a bit higher than the simulation results at low SNRs, especially for the $(2, 1)$ and $(2, 2)$ systems. As the SNR or the number of RAs increases, the upper-bounds agree with the simulation results very well.

Moreover, both the numerical results of the upper-bounds and the simulation results substantiate that the BER performance of the BPSK-modulated DBSM is about 1dB better than that of the conventional SM. The main reason behind this is that the overall Euclidean distance between two DBSM-formed signals is larger than that between two conventional SM-formed signals in the same configuration. As shown by the shaded cells in Table 6, $\mathbf{d}_{l,l'}^{k,k'} = 2\mathbf{h}_m \sim \mathcal{CN}(\mathbf{0}_{N \times 1}, 4\mathbf{I}_N)$, $m = 1, 2$, for the number of different bits in a pair of DBSM-formed signals, $N_{l \to l'}^{k \to k'} = 2$, while $\mathbf{q}_{m,m'}^{k,k'} = \mathbf{h}_1 + \mathbf{h}_2 \sim \mathcal{CN}(\mathbf{0}_{N \times 1}, 2\mathbf{I}_N)$ for the number of different bits in a pair of conventional SM-formed signals, $N_{m \to m'}^{k \to k'} = 2$. More specifically, the Euclidean distance between the DBSM signals mapped by 00 and 11 is $\|2\mathbf{h}_1\|$, and that between the DBSM signals mapped by 01 and 10 is $\|2\mathbf{h}_2\|$. By contrast, the Euclidean distance between the conventional SM signals mapped by 00 and 11 or 01 and 10 is $\|\mathbf{h}_1 + \mathbf{h}_2\|$.

Since $\mathcal{E}\{\|\mathbf{d}_{l,l'}^{k,k'}\|^2\} = 2\mathcal{E}\{\|\mathbf{q}_{m,m'}^{k,k'}\|^2\}$ for $N_{l \to l'}^{k \to k'} = N_{m \to m'}^{k \to k'} = 2$, the DBSM guarantees the largest mean Euclidean distance $\mathcal{E}\{\|2\mathbf{h}_m\|\}$, $m \in \{1, 2\}$, pertaining to the largest number of different bits, $2 \log_2 M = 2$, in BPSK-modulated systems. In (22) and (23), the Q-function is a monotonically decreasing function and, accordingly, we have $Q(\|\mathbf{d}_{l,l'}^{k,k'}\|/\sqrt{2\sigma_Z^2}) < Q(\|\mathbf{q}_{m,m'}^{k,k'}\|/\sqrt{2\sigma_Z^2})$ for the case

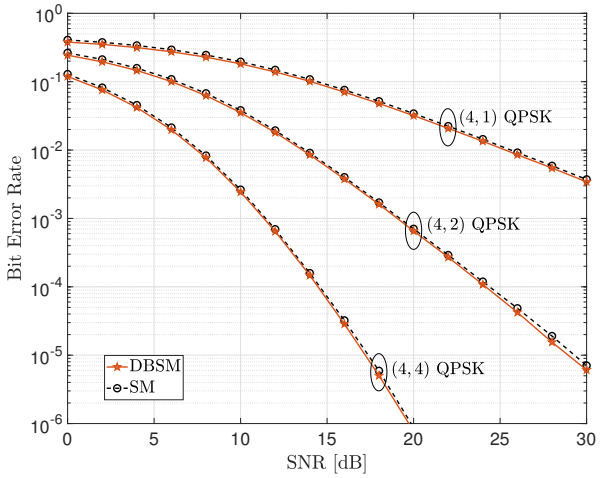

FIGURE 7. BER comparisons between DBSM and conventional SM in QPSK-modulated $(4, 1)$, $(4, 2)$, and $(4, 4)$ systems.

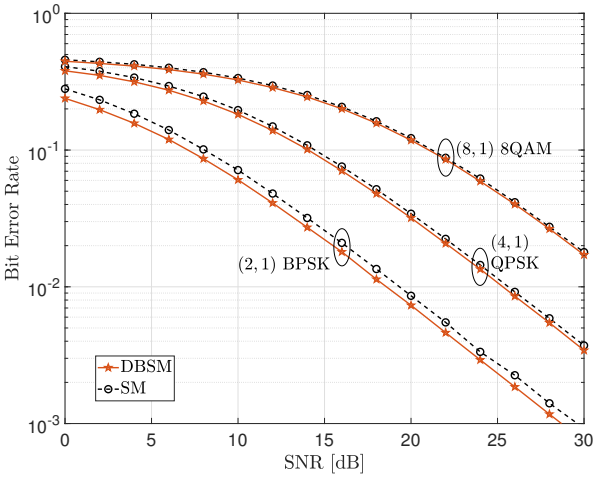

FIGURE 8. The impact of increasing M on the performance gain achieved by DBSM over conventional SM.

of $N_{l\to l'}^{k\to k'} = N_{m\to m'}^{k\to k'} = 2$ from an ergodic perspective, which leads to the DBSM having higher reliability than the conventional SM.

In the same way, the largest mean Euclidean distance $\mathcal{E}\{\|2\mathbf{h}_m\|\}$, $m \in \{1, 2, 3, 4\}$, is guaranteed by the QPSK-modulated DBSM for the case that $N_{l\to l'}^{k\to k'} = 4$, which can be observed from Table 7. In the case that $N_{m\to m'}^{k\to k'} = 4$, the mean Euclidean distance between two conventional SM-formed signals is $\mathcal{E}\{\|\mathbf{h}_m + \mathbf{h}_{m'}\|\}$, where $m, m' = 1, 2, 3, 4$ and $|m - m'| = 2$. The BERs of the DBSM and the conventional SM are compared in Fig. 7 for the QPSK-modulated $(4, 1)$, $(4, 2)$, and $(4, 4)$ systems, where the DBSM achieves better BER performance. Explicitly, the performance gain achieved by the QPSK-modulated DBSM over the conventional SM is smaller than that achieved by the BPSK-modulated DBSM. This is because of the following two reasons. Firstly, the proportion of the bit-sequence pairs having the largest number of different bits, $2\log_2 M$, in all the pairs is $1/M^2$, which gets lower as M increases. Secondly, the difference between $Q(\|2\mathbf{h}_m\|/\sqrt{2\sigma_Z^2})$ for the largest number of different bits and $(2\log_2 M - 1)/(2\log_2 M)Q(\|\mathbf{h}_m + \mathbf{h}_{m'}\|/\sqrt{2\sigma_Z^2})$ for the second largest number scenario becomes negligible, as M increases. As such, the contribution of the bit-sequence pairs having the largest number of different bits to the summation in the BER (22) is reduced upon increasing M, which shrinks the performance gain achieved by the DBSM over the conventional SM.

To further expose the impact of increasing M on the performance gain of the DBSM, Fig. 8 compares the BERs of the DBSM and the conventional SM in $(2, 1)$, $(4, 1)$, and $(8, 1)$ systems. From Figs. 6 and 7, we may find that the performance gain achieved by the DBSM over the conventional SM remains the same with the increase in the number of RAs, N. Therefore, the performance with more RAs can be anticipated in a straightforward manner based on the case of $N = 1$ investigated in Fig. 8. As shown in this figure, the performance gain of the DBSM is reduced as M increases. The main reason behind this is that all the bit-sequence pairs appear at the same probability, and the contribution of the pairs having the largest number of different bits to the BER reduction is degraded upon increasing M, as justified in the discussion on Fig. 7. More specifically, the DBSM systems with $M = 2$, 4, and 8 achieve nearly 1dB, 0.6dB and 0.3dB performance gains, respectively, over the conventional SM systems with the same configurations.

B. CHANNEL-CODED SYSTEMS

Herein, channel coding techniques are applied to the DBSM for augmenting the DBSM's advantage in the largest mean Euclidean distance imposed upon a pair of complementary bit-sequences. For the information delivery over physical channels, the Hamming distance between two codewords is reflected by the Euclidean distance between the signals mapped by the codewords. Thus, channel coding will boost the performance gain achieved by the DBSM over the conventional SM.

1) Convolutional Coding

The block diagram of a DBSM system relying on convolutional coding is shown in Fig. 9. The counterpart of a conventional SM system using convolutional coding can be obtained directly upon replacing the circled DBSM modules by conventional SM modules.

A popular convolutional encoder having a constraint length of 7 and code rate of $1/2$ is used as an example for illustrating the performance gain of the DBSM. The generator polynomials are $1 + u^{-1} + u^{-2} + u^{-3} + u^{-6}$ and $1 + u^{-2} + u^{-3} + u^{-5} + u^{-6}$. A hard-decision Viterbi decoder having 64 states is utilised at the receiver for decoding. A

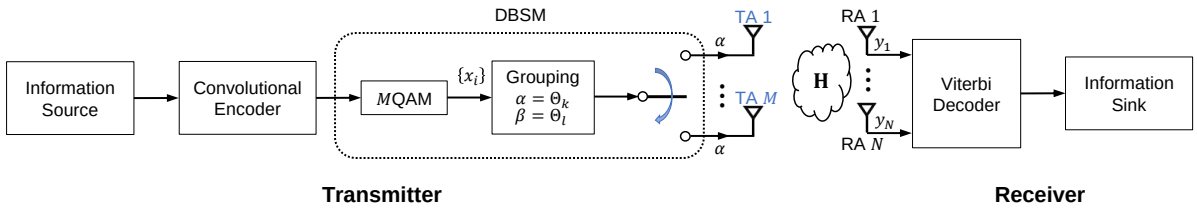

FIGURE 9. **A DBSM system with convolutional coding.**

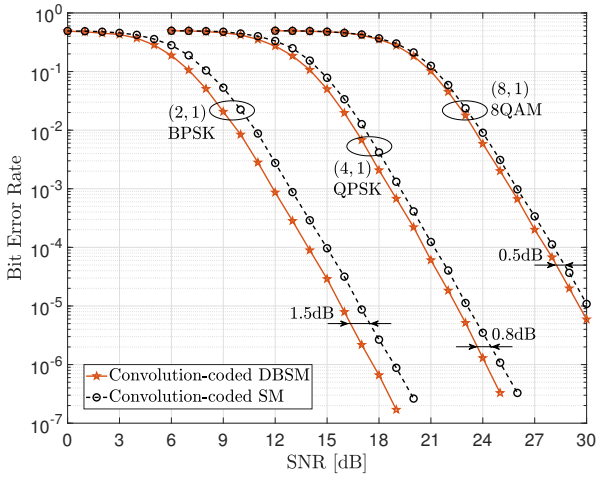

FIGURE 10. **BER comparisons between DBSM and conventional SM in $(2,1)$, $(4,1)$, and $(8,1)$ systems with convolutional coding.**

frame is composed of 2436 information bits. With 12 tail bits added for the trellis termination, there are 4884 bits in the resultant codeword. For each BER measurement, 10^5 frames are used for evaluating the statistics at a SNR in a given system configuration.

The BERs of DBSM and conventional SM using convolutional coding are compared in Fig. 10 for BPSK-modulated $(2,1)$, QPSK-modulated $(4,1)$ and 8QAM-modulated $(8,1)$ systems. Compared to the BERs of uncoded systems in Fig. 8, the channel-coded systems significantly enhance the performance gain achieved by the DBSM over the conventional SM, as shown in Fig. 10. The main reason behind this is that complementary channel-coded bit-sequences tend to appear in any pair of codewords at a near-unity probability. By contrast, in uncoded systems all pairs of bit-sequences tend to appear at a similar probability. As a benefit of channel coding, the above observation results in a higher probability for the largest Euclidean distance sequences to be picked by the channel-coded DBSM, than in uncoded systems.

To elaborate briefly, the computational complexity of the hard-decision Viterbi decoder in a DBSM system is exactly the same as that in a conventional SM system of the same configuration. Given this condition, for $M = 2$, 4, and 8, the DBSM systems using convolutional coding achieve 1.5dB, 0.8dB and 0.5dB performance gains, respectively, over the conventional SM systems with convolutional coding.

2) Turbo Coding

The block diagram of a turbo-coded DBSM system is shown in Fig. 11. The counterpart of a turbo-coded conventional SM system can be obtained directly by replacing the circled DBSM modules with the conventional SM modules.

The turbo coding scheme used in the long-term evolution (LTE) standard is adopted in our simulations. A frame is composed of 2432 information bits, and the base rate is $1/3$. The output of the turbo encoder is composed of three streams: one contains systematic bits, and the other two contain parity bits. The interleaver permutes the indices of the input bits based on a quadratic polynomial permutation [25]. The feed-forward and the feedback generator polynomials are expressed as $1 + u^{-2} + u^{-3}$ and $1 + u^{-1} + u^{-3}$, respectively, which are used to generate the two parity bit streams [26]. With 4 tail bits added at each stream for the trellis termination, the resultant length of a codeword is $(2432 + 4) \times 3 = 7038$.

The codewords are modulated either by the DBSM or by the conventional SM, and then delivered through the physical channels. At the receiver, the soft decision is used for obtaining the log–likelihood ratio (LLR) of each bit in a received codeword, calculated as [27]

$$LLR(v_i) = \ln \frac{\sum_{v_i=0} \exp\left(-\frac{\|\mathbf{y}(v_i) - \mathbf{h}_{\sharp v_i}\Theta(v_i)\|^2}{\sigma_Z^2}\right)}{\sum_{v_i=1} \exp\left(-\frac{\|\mathbf{y}(v_i) - \mathbf{h}_{\sharp v_i}\Theta(v_i)\|^2}{\sigma_Z^2}\right)}, \quad (24)$$

where v_i is the i^{th} bit in a codeword, $i = 1, 2, \cdots, 7038$, and the $N \times 1$ vector $\mathbf{y}(v_i)$ contains the received signals given the bit v_i in its position. The $N \times 1$ vector $\mathbf{h}_{\sharp v_i} \in \{\mathbf{h}_1, \mathbf{h}_2, \cdots, \mathbf{h}_M\}$ contains the channel coefficients of the links spanning from the TA activated by the bit v_i to all the RAs, and the TA is activated according to the DBSM or the conventional SM design. The MQAM symbol $\Theta(v_i) \in \{\Theta_0, \Theta_1, \cdots, \Theta_{M-1}\}$ is mapped by the bit-sequence with v_i in its position.

We remark that the computational complexity of the soft decision in an DBSM system is exactly the same as that in a conventional SM system, i.e., associated with M^2 multiplications and $2M^2 \log_2 M$ additions for the calculation of each LLR. Using the LLRs of all the 7038 bits in a received codeword, the turbo decoding is performed to get the 2432 decoded information bits of a frame. For each BER

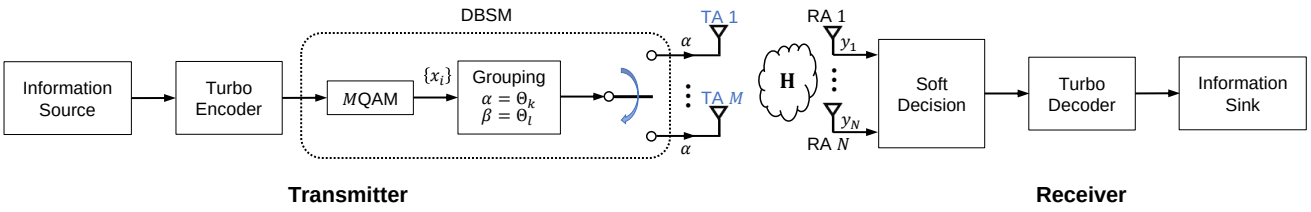

FIGURE 11. **A turbo-coded DBSM system.**

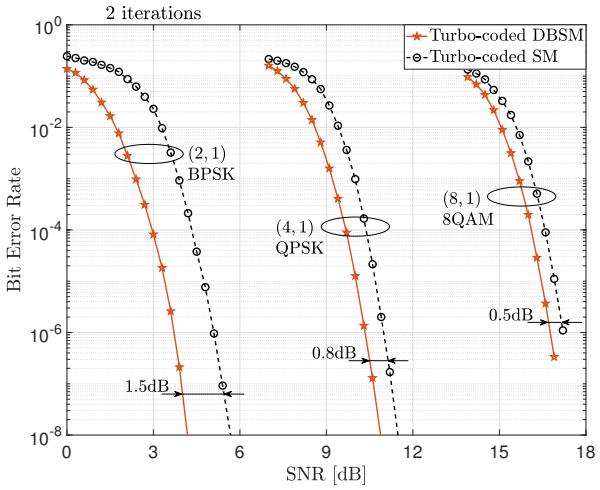

(a) 2 iterations in turbo decoding

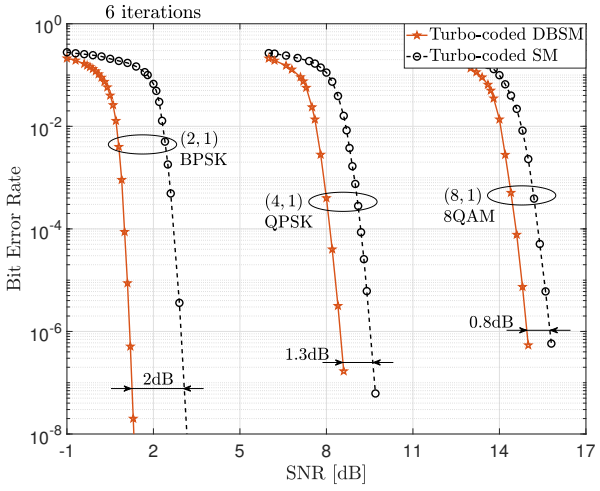

(b) 6 iterations in turbo decoding

FIGURE 12. **BER comparisons between DBSM and conventional SM in turbo-coded $(2,1)$, $(4,1)$, and $(8,1)$ systems.**

measurement at a SNR in a given system configuration, 10^5 frames are conveyed to get the statistics.

The BERs of turbo-coded DBSM and turbo-coded conventional SM are compared in Fig. 12 for BPSK-modulated $(2,1)$, QPSK-modulated $(4,1)$, and 8QAM-modulated $(8,1)$ systems, where the turbo decoder executing 2 iterations and that executing 6 iterations are used in each system to characterise the performance-versus-complexity tradeoff. As shown in this figure, the performance gain achieved by the DBSM over the conventional SM is significantly enhanced in turbo-coded systems, compared to that in the uncoded systems. Moreover, the performance gain achieved by the DBSM over the conventional SM is further increased when a more powerful decoder is utilised. More specifically, upon executing 2 iterations in the decoding, the turbo-coded DBSM systems with $M = 2$, 4, and 8 achieve 1.5dB, 0.8dB and 0.5dB performance gains, respectively, over the turbo-coded conventional SM systems having the same configurations. These performance gains are 2dB, 1.3dB and 0.8dB, respectively, if 6 iterations are executed. This reveals that the engagement of more powerful decoders will better exploit the advantages of our DBSM design.

V. CONCLUSION

A. SUMMARY

In this paper, a new multi-antenna transmission scheme, referred to as DBSM, has been proposed to improve the reliability of SM. In each DBSM transmission, two MQAM symbols are conveyed in different ways. One is physically radiated from an active TA, which is selected according to the difference between the two symbols. Although the other one is not radiated physically, its information is carried by the radiated one and the specific selection of the active TA.

The benefit of the DBSM lies in the TA indexing and the MQAM mapping, which ensures that the largest possible Euclidean distance is applied to a pair of DBSM signals that are mapped by complementary bit-sequences. This guarantees that the DBSM outperforms the conventional SM, especially with the aid of channel coding techniques.

Our theoretical analysis and illustrative simulation results have substantiated that DBSM has the following energy-efficiency, spectral-efficiency, and reliability advantages:

(i) Similar with conventional SM, DBSM requires only a single RF chain as it activates only a single TA in each transmission. This improves the energy efficiency and avoids inter-channel and/or inter-antenna interference.

(ii) The DBSM utilises a single TA to radiate a single symbol in each transmission, which guarantees that there is no inter-symbol interference at all in the simultaneous delivery of two symbols. In terms of the ADR, the spectral efficiency of the DBSM is the same as that of the conventional SM, given the same system

configuration. In particular, the DBSM achieves full spatial multiplexing gain in BPSK-modulated systems having two TAs.

(iii) As the DBSM imposes the largest possible Euclidean distance on the delivery of two complementary bit-sequences, it achieves higher reliability than the conventional SM. The performance gain achieved by DBSM over conventional SM in the coded systems is higher than that of uncoded systems, because complementary bit-sequence pairs appear at higher probability when using channel coding techniques.

B. FUTURE WORK

We introduced the DBSM concept and its constellation design. Furthermore, we characterised its performance in terms of ADR and BER.

Since the idea of SM has opened the door for information mapping through various dimensions, e.g., frequency bands, time slots, spreading codes, and dispersion matrices, our DBSM can also be applied to those dimensions in a straightforward manner. Moreover, advanced channel coding and signal detection solutions are being pursued to further improve the DBSM performance, specifically for higher-order modulated massive MIMO systems.

REFERENCES

[1] Y. Yang, M. Guizani and B. Jiao, "Difference Based Spatial Modulation", *Proc. Int. Wireless Commun. Mobile Comput. Conf. (IWCMC)*, pp. 295-299, May 2022.

[2] M. Vaezi, *et al.*, "Cellular, Wide-Area, and Non-Terrestrial IoT: A Survey on 5G Advances and the Road Toward 6G", *IEEE Commun. Surveys Tuts.*, vol. 24, no. 2, pp. 1117-1174, 2nd Quart., 2022.

[3] P. Popovski, *et al.*, "A Perspective on Time Toward Wireless 6G", *Proc. IEEE*, vol. 110, no. 8, pp. 1116-1146, Aug. 2022.

[4] N. Ishikawa, S. Sugiura, and L. Hanzo, "50 years of permutation, spatial and index modulation: From classic RF to visible light communications and data storage", *IEEE Commun. Surveys Tuts.*, vol. 20, no. 3, pp. 1905-1938, 3rd Quart., 2018.

[5] S. Tusha, A. Tusha, E. Basar and H. Arslan, "Multidimensional Index Modulation for 5G and Beyond Wireless Networks", *Proc. IEEE*, vol. 109, no. 2, pp. 170-199, Feb. 2021.

[6] P. Yang, M. Di Renzo, Y. Xiao, S. Li and L. Hanzo, "Design guidelines for spatial modulation", *IEEE Commun. Surveys Tuts.*, vol. 17, no. 1, pp. 6-26, 1st Quart., 2015.

[7] Y. Yang and B. Jiao, "Information-guided channel-hopping for high data rate wireless communication", *IEEE Commun. Lett.*, vol. 12, no. 4, pp. 225-227, Apr. 2008.

[8] Y. Yang, N. Bonello, and S. Aissa, "An information-guided channel-hopping scheme for block-fading channels with estimation errors", in *Proc. IEEE Global Commun. Conf.*, Dec. 2010.

[9] Y. Yang and S. Aissa, "Information guided communications in MIMO systems with channel state impairments", *Wireless Commun. Mobile Comput.*, vol. 15, no. 5, pp. 868-878, Apr. 2015.

[10] C. Liu, M. Ma, Y. Yang, and B. Jiao, "Optimal spatial-domain design for spatial modulation capacity maximization", *IEEE Commun. Lett.*, vol. 20, no. 6, pp. 1092-1095, Jun. 2016.

[11] Y. Shi, M. Ma, Y. Yang, and B. Jiao, "Optimal power allocation in spatial modulation systems", *IEEE Trans. Wireless Commun.*, vol. 16, no. 3, pp. 1646-1655, Mar. 2017.

[12] Y. Yang and S. Aissa, "Bit-padding information guided channel hopping", *IEEE Commun. Lett.*, vol. 15, no. 2, pp. 163-165, Feb. 2011.

[13] Y. Yang and S. Aissa, "Information guided channel hopping with an arbitrary number of transmit antennas", *IEEE Commun. Lett.*, vol. 16, no. 10, pp. 1552-1555, Oct. 2012.

[14] A. Jaiswal, M. Abaza, M. Bhatnagar, and V. Jain, "An investigation of performance and diversity property of optical space shift keying-based FSO-MIMO system", *IEEE Trans. Commun.*, vol. 66, no. 9, pp. 4028-4042, Sep. 2018.

[15] H. Olanrewaju, J. Thompson, and W. Popoola, "Performance of optical spatial modulation in indoor multipath channel", *IEEE Trans. Wireless Commun.*, vol. 17, no. 9, pp. 6042-6052, Sep. 2018.

[16] Y. Yang and M. Guizani, "Mapping-varied spatial modulation for physical layer security: Transmission strategy and secrecy rate", *IEEE J. Sel. Areas Commun.*, vol. 36, no. 4, pp. 877-889, Apr. 2018.

[17] Y. Yang, M. Ma, S. Aissa, and L. Hanzo, "Physical-layer secret key generation via CQI-mapped spatial modulation in multi-hop wiretap *ad-hoc* networks", *IEEE Trans. Inf. Forensics Security*, vol. 16, pp. 1322-1334, 2021.

[18] E. Basar, "Reconfigurable intelligent surface-based index modulation: A new beyond MIMO paradigm for 6G", *IEEE Trans. Commun.*, vol. 68, no. 5, pp. 3187-3196, May 2020.

[19] Q. Li, M. Wen and M. Di Renzo, "Single-RF MIMO: From spatial modulation to metasurface-based modulation", *IEEE Wireless Commun.*, vol. 28, no. 4, pp. 88-95, Aug. 2021.

[20] S. Sugiura, S. Chen and L. Hanzo, "Coherent and differential space–time shift keying: A dispersion matrix approach", *IEEE Trans. Commun.*, vol. 58, no. 11, pp. 3219-3230, Nov. 2010.

[21] Y. Bian, X. Cheng, M. Wen, L. Yang, H. V. Poor and B. Jiao, "Differential spatial modulation", *IEEE Trans. Veh. Technol.*, vol. 64, no. 7, pp. 3262-3268, Jul. 2015.

[22] L. Zheng and D. N. C. Tse, "Diversity and multiplexing: a fundamental tradeoff in multiple-antenna channels," *IEEE Trans. Inf. Theory*, vol. 49, no. 5, pp. 1073-1096, May 2003.

[23] G. Foschini, "Layered space-time architecture for wireless communication in a fading environment when using multi-element antennas", *Bell Labs Tech. J.*, vol. 1, no. 2, pp. 41-59, 1996.

[24] A. J. Goldsmith, *Wireless Communications*, Cambridge University Press, 2005.

[25] M. Brejza, *et al.*, "20 Years of Turbo Coding and Energy-Aware Design Guidelines for Energy-Constrained Wireless Applications", *IEEE Commun. Surveys Tuts.*, vol. 18, no. 1, pp. 8-28, 1st Quart. 2016.

[26] H. Zarrinkoub, *Understanding LET with MATLAB*, John Wiley & Sons, 2014, Ch. 4.4, pp. 85-93.

[27] S. Sugiura, S. Chen and L. Hanzo, "MIMO-Aided Near-Capacity Turbo Transceivers: Taxonomy and Performance versus Complexity", *IEEE Commun. Surveys Tuts.*, vol. 14, no. 2, pp. 421-442, 2nd Quart. 2012.

Yuli Yang (Senior Member, IEEE) received the Ph.D. degree in communications and information systems from Peking University, Beijing, China, in July 2007. Her industry experience includes working with Huawei Technologies, Beijing, China, as an Intern Researcher from June 2006 to July 2007, and with Bell Labs, Shanghai, China, as a Research Scientist from August 2007 to December 2009. From January 2010 to March 2023, she was with King Abdullah University of Science & Technology, Thuwal, Saudi Arabia; Melikşah University, Talas, Turkey; the University of Chester, Chester, U.K.; the University of Lincoln, Lincoln, U.K., on various academic positions.

Since March 2023, she has been with the University of Essex, Colchester, U.K., as a Senior Lecturer in Communications and Networks. Her research interests include modeling, design, analysis, and optimization of wireless systems and networks, specifically in physical-layer security, permutation-based modulation/transmission, and ultrareliable low-latency communications.

Chao Xu (Senior Member, IEEE) received a B.Eng. degree from Beijing University of Posts and Telecommunications, China, and a BSc(Eng) with First Class Honours from Queen Mary, University of London, UK, through a Sino-UK joint degree program in 2008, both in Telecommunications. He obtained a MSc degree with distinction in Radio Frequency Communication Systems and a Ph.D. degree in Wireless Communications from the University of Southampton, UK in 2009 and 2015, respectively. He is currently a senior research fellow working at Next Generation Wireless Research Group, University of Southampton, UK. His research interests include index modulation, reconfigurable intelligent surfaces, noncoherent detection and turbo detection. He was awarded the Best M.Sc. Student in Broadband and Mobile Communication Networks by the IEEE Communications Society (United Kingdom and Republic of Ireland Chapter) in 2009. He also received 2012 Chinese Government Award for Outstanding Self-Financed Student Abroad and 2017 Dean's Award, Faculty of Physical Sciences and Engineering, the University of Southampton.

Lajos Hanzo (Life Fellow, IEEE) received Honorary Doctorates from the Technical University of Budapest (2009) and Edinburgh University (2015). He is a Foreign Member of the Hungarian Science-Academy, Fellow of the Royal Academy of Engineering (FREng), of the IET, of EURASIP and holds the IEEE Eric Sumner Technical Field Award. (http://www-mobile.ecs.soton.ac.uk, https://en.wikipedia.org/wiki/Lajos_Hanzo)